scientific reports

Check for updates

OPEN

Characteristic parameters of photonic nanojets of single dielectric microspheres illuminated by focused broadband radiation

Amartya Mandal[1,3], Pragya Tiwari[1,3], Paul K. Upputuri[2] & Venkata R. Dantham[1]✉

Herein, we report the theoretical investigation on the photonic nanojets (PNJs) of single dielectric microspheres illuminated by focused broadband radiation (polychromatic light) from a Halogen lamp, supercontinuum source, light-emitting diode, and Hg arc lamp. The role of incident beam waist, refractive index of the surrounding medium, and radius of the microsphere on the characteristic parameters such as the electric field intensity enhancement, effective width, and length of the PNJ is studied. Interestingly, the characteristic parameters of the PNJs of solid microspheres obtained for the above-mentioned broadband radiation sources are found close to those observed for the focused monochromatic radiation of wavelengths which are near to the central wavelengths of the sources. Moreover, the characteristic parameters of PNJs of the core–shell microspheres of different thicknesses (*t*) illuminated by polychromatic radiation from most commonly used sources such as Halogen and Hg arc lamps are studied. For each *t* value, a suitable wavelength of monochromatic radiation has been found to generate the PNJ with characteristic parameters which are close to those obtained in the case of polychromatic radiation. We believe that the analytical theory and the theoretical simulations reported here would be useful for researchers who work in the fields such as PNJ assisted photoacoustic spectroscopy, white light nanoscopy, low-coherence phase-shifting interference microscopy, and Mirau interferometry.

Transparent dielectric single microspheres support optical resonances or whispering gallery modes upon the resonant light illumination[1–3]. The quality factor of these resonances is improved significantly when the microspheres are excited with suitable geometries[4–8]. The microspheres are also found to support super-resonances for specific values of size parameters[9,10]. However, narrow-focused and intense electromagnetic beams are generated at the shadow side of these microspheres upon the non-resonant light illumination. These are non-evanescent beams and are named 'photonic nanojets' (PNJs)[11–17]. These PNJs are generated from solid/core–shell dielectric microparticles illuminated by a plane wave[18,19], spherical wave[20], Gaussian beam[21,22], Bessel beam[23,24], etc. The origin of the PNJ is explained based on the forward Mie scattering and focused near-field diffraction[25–27].

It is to be noted that the PNJs generated by monochromatic light are found useful for enhancing Raman scattering[28–31], fluorescence signals[32], nanoparticles sensing[33], optical data storage[34], laser surgery[35], optical transport[36], two-photon fluorescence[37], nanolithography[38], biomedical research[39] etc. On the other hand, several researchers have generated the PNJs using the focused polychromatic light used for enhancing the backscattering signals of nanoparticles[40], photoacoustic spectroscopy[41], white light nanoscopy[42–49], low-coherence phase-shifting interference microscopy[50], Mirau interferometry[51], and super-resolution imaging[52–54]. It is worth mentioning here that several theoretical studies are reported on PNJs of single microspheres illuminated by monochromatic plane and Gaussian waves[18,55–59]. The role of key parameters such as incident beam waist (ω_0), refractive index of the surrounding medium (n_m), radius (R_s), and refractive index (n_s) of the microspheres on the characteristic parameters of the PNJs is reported in detail. Few theoretical studies related to the PNJs of single dielectric microspheres under pulsed irradiation (or coherent broadband illumination) are also reported in the literature[60,61]. Under the pulsed irradiation, the PNJs appear to be non-stationary and these are found useful in micromachining beyond the diffraction limit[62], microscopy[63], and non-linear optics[64]. However, details of the characteristic parameters of the PNJs generated by focused polychromatic light (or broadband radiation) and the role of R_s, n_m, and ω_0 on

[1]Department of Physics, Indian Institute of Technology Patna, Daulatpur, Bihar 801103, India. [2]School of Chemical and Biomedical Engineering, Nanyang Technological University, 62 Nanyang Drive, Singapore 637459, Singapore. [3]These authors contributed equally: Amartya Mandal and Pragya Tiwari. ✉email: dantham@iitp.ac.in

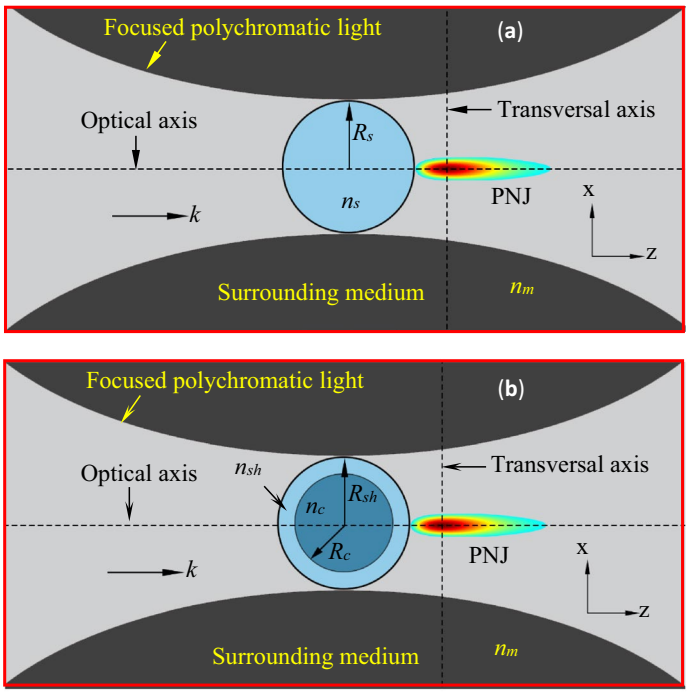

Figure 1. Illustration of PNJs generated by single solid microsphere (panel a) and core–shell microsphere (panel b) under focused polychromatic illumination. Here R_s, R_c, and R_{sh} are the radii of the solid microsphere, core, and shell, respectively. n_s, n_c, n_{sh}, and n_m are the refractive indices of the solid microsphere, core, shell, and surrounding medium, respectively.

the characteristic parameters of the PNJs generated by broadband radiation are not reported in the literature. Moreover, the differences in the PNJs generated by focused monochromatic light and polychromatic light are not reported. These details would be useful for optimizing the experimental signals obtained using PNJs generated by polychromatic light. Therefore, we have performed a theoretical investigation on the PNJ of single solid and core–shell microspheres illuminated by focused polychromatic light from different sources.

Herein, we report (1) the electric field intensity enhancement (EFIE) distribution inside and outside single dielectric microspheres illuminated by polychromatic light from different light sources such as Hg arc lamp, white LED, supercontinuum (SC) source, and Halogen lamp, (2) the role of ω_0, R_s, and n_m on the characteristic parameters of PNJs obtained for polychromatic illumination, (3) the characteristic parameters of the PNJs of single microspheres illuminated by monochromatic light, (4) the EFIE distribution inside and outside core–shell microspheres under monochromatic and polychromatic illumination.

Theoretical aspects

Recently, we have developed an analytical theory for estimating the electric field enhancement inside and outside single core–shell dielectric microspheres illuminated by focused monochromatic light[59]. Using this theory, the characteristic parameters of the PNJs generated by core–shell microspheres of different sizes and refractive indices are estimated. In the present study, the analytical theory has been extended to study the characteristic parameters of the PNJs of single solid/core–shell microspheres illuminated by focused polychromatic light (Fig. 1) from different sources.

The final expressions for plotting the EFIE in the surrounding medium (η_m), core (η_c), and shell (η_{sh}) are given below.

$$\eta_m = \sum_{p=1}^{k} I_m(r, \theta, \phi, \lambda_p) \tag{1}$$

$$\eta_c = \sum_{p=1}^{k} I_c(r, \theta, \phi, \lambda_p) \tag{2}$$

$$\eta_{sh} = \sum_{p=1}^{k} I_{sh}(r, \theta, \phi, \lambda_p) \tag{3}$$

$$I_m(r, \theta, \phi, \lambda_p) = E_{r,m}^2 + E_{\theta,m}^2 + E_{\phi,m}^2 \tag{4}$$

$$I_c(r,\theta,\phi,\lambda_p) = E_{r,c}^2 + E_{\theta,c}^2 + E_{\phi,c}^2 \tag{5}$$

$$I_{sh}(r,\theta,\phi,\lambda_p) = E_{r,sh}^2 + E_{\theta,sh}^2 + E_{\phi,sh}^2 \tag{6}$$

here (r,θ,ϕ) are the spherical polar coordinates. $\lambda_1, \lambda_2, \lambda_3, \ldots, \lambda_k$ represent different wavelengths present in the polychromatic light. $E_{r,m}$, $E_{r,c}$, and $E_{r,sh}$ are the enhancements in the radial component of the electric field in the medium, core, and shell, respectively. $E_{\theta,m}$, $E_{\theta,c}$, and $E_{\theta,sh}$ are the enhancements in the angular component of the electric field in the medium, core, and shell, respectively. $E_{\phi,m}$, $E_{\phi,c}$, and $E_{\phi,sh}$ are the enhancements in the azimuthal component of the electric field in the medium, core, and shell, respectively. These components can be estimated using the following expressions.

$$E_{r,m} = E_p(\lambda_p)\cos\phi \sum_{n=1}^{\infty} C_n g_n a_n^m(\lambda_p)\left[\xi_n''(k_m(\lambda_p)r) + \xi_n(k_m(\lambda_p)r)\right]P_n^1(\cos\theta) \tag{7}$$

$$E_{\theta,m} = \frac{E_p(\lambda_p)}{k_m(\lambda_p)r}\cos\phi \sum_{n=1}^{\infty} C_n g_n\left[a_n^m(\lambda_p)\xi_n'(k_m(\lambda_p)r)\tau_n(\cos\theta) - ib_n^m(\lambda_p)\xi_n(k_m(\lambda_p)r)\pi_n(\cos\theta)\right] \tag{8}$$

$$E_{\phi,m} = -\frac{E_p(\lambda_p)}{k_m(\lambda_p)r}\sin\phi \sum_{n=1}^{\infty} C_n g_n\left[a_n^m(\lambda_p)\xi_n'(k_m(\lambda_p)r)\pi_n(\cos\theta) - ib_n^m(\lambda_p)\xi_n(k_m(\lambda_p)r)\tau_n(\cos\theta)\right] \tag{9}$$

$$E_{r,sh} = -E_p(\lambda_p)\cos\phi \sum_{n=1}^{\infty} C_n g_n \left\{ \begin{array}{l} a_n^{sh\alpha}(\lambda_p)\left[\psi_n''(k_{sh}(\lambda_p)r) + \psi_n(k_{sh}(\lambda_p)r)\right] \\ -a_n^{sh\beta}(\lambda_p)\left[\xi_n''(k_{sh}(\lambda_p)r) + \xi_n(k_{sh}(\lambda_p)r)\right] \end{array} \right\} P_n^1(\cos\theta) \tag{10}$$

$$E_{\theta,sh} = -\frac{E_p(\lambda_p)}{k_{sh}(\lambda_p)r}\cos\phi \sum_{n=1}^{\infty} C_n g_n \left\{ \begin{array}{l} \left[a_n^{sh\alpha}(\lambda_p)\psi_n'(k_{sh}(\lambda_p)r) - a_n^{sh\beta}(\lambda_p)\xi_n'(k_{sh}(\lambda_p)r)\right]\tau_n(\cos\theta) \\ -i\left[b_n^{sh\alpha}(\lambda_p)\psi_n(k_{sh}(\lambda_p)r) - b_n^{sh\beta}(\lambda_p)\xi_n(k_{sh}(\lambda_p)r)\right]\pi_n(\cos\theta) \end{array} \right\} \tag{11}$$

$$E_{\phi,sh} = \frac{E_p(\lambda_p)}{k_{sh}(\lambda_p)r}\sin\phi \sum_{n=1}^{\infty} C_n g_n \left\{ \begin{array}{l} \left[a_n^{sh\alpha}(\lambda_p)\psi_n(k_{sh}(\lambda_p)r) - a_n^{sh\beta}(\lambda_p)\xi_n(k_{sh}(\lambda_p)r)\right]\pi_n(\cos\theta) \\ -i\left[b_n^{sh\alpha}(\lambda_p)\psi_n'(k_{sh}(\lambda_p)r) - b_n^{sh\beta}(\lambda_p)\xi_n'(k_{sh}(\lambda_p)r)\right]\tau_n(\cos\theta) \end{array} \right\} \tag{12}$$

$$E_{r,c} = -E_p(\lambda_p)\cos\phi \sum_{n=1}^{\infty} C_n g_n a_n^c(\lambda_p)\left[\psi_n''(k_c(\lambda_p)r) + \psi_n(k_c(\lambda_p)r)\right]P_n^1(\cos\theta) \tag{13}$$

$$E_{\theta,c} = -\frac{E_p(\lambda_p)}{k_c(\lambda_p)r}\cos\phi \sum_{n=1}^{\infty} C_n g_n\left[a_n^c(\lambda_p)\psi_n'(k_c(\lambda_p)r)\tau_n(\cos\theta) - ib_n^c(\lambda_p)\psi_n(k_c(\lambda_p)r)\pi_n(\cos\theta)\right] \tag{14}$$

$$E_{\phi,c} = \frac{E_p(\lambda_p)}{k_c(\lambda_p)r}\sin\phi \sum_{n=1}^{\infty} C_n g_n\left[a_n^c(\lambda_p)\psi_n'(k_c(\lambda_p)r)\pi_n(\cos\theta) - ib_n^c(\lambda_p)\psi_n(k_c(\lambda_p)r)\tau_n(\cos\theta)\right] \tag{15}$$

$$C_n = \mathrm{i}^{(n+1)}(-1)^n\frac{2n+1}{n(n+1)} \tag{16}$$

$$a_n^m(\lambda_p) = X_3/X_1;\ a_n^c(\lambda_p) = X_4/X_1;\ a_n^{sh\alpha}(\lambda_p) = X_5/X_1;\ a_n^{sh\beta}(\lambda_p) = X_6/X_1 \tag{17}$$

$$b_n^m(\lambda_p) = X_7/X_2;\ b_n^c(\lambda_p) = X_4/X_2;\ b_n^{sh\alpha}(\lambda_p) = X_8/X_2;\ b_n^{sh\beta}(\lambda_p) = X_9/X_2 \tag{18}$$

$$\begin{aligned} X_1 = {} & n_{sh}^2\xi'(k_m(\lambda_p)R_{sh})\psi'(k_c(\lambda_p)R_c)M_1 + n_m n_c\xi(k_m(\lambda_p)R_{sh})\psi(k_c(\lambda_p)R_c)M_2 \\ & + n_{sh}n_c\xi'(k_m(\lambda_p)R_{sh})\psi(k_c(\lambda_p)R_c)M_3 + n_m n_{sh}\xi(k_m(\lambda_p)R_{sh})\psi'(k_c(\lambda_p)R_c)M_4 \end{aligned} \tag{19}$$

$$\begin{aligned} X_2 = {} & n_m n_c\xi'(k_m(\lambda_p)R_{sh})\psi'(k_c(\lambda_p)R_c)M_1 + n_{sh}^2\xi(k_m(\lambda_p)R_{sh})\psi(k_c(\lambda_p)R_c)M_2 \\ & + n_m n_{sh}\xi'(k_m(\lambda_p)R_{sh})\psi(k_c(\lambda_p)R_c)M_3 + n_{sh}n_c\xi(k_m(\lambda_p)R_{sh})\psi'(k_c(\lambda_p)R_c)M_4 \end{aligned} \tag{20}$$

$$X_3 = n_{sh}^2\psi'(k_c(\lambda_p)R_c)\psi'(k_m(\lambda_p)R_{sh})M_1 + n_c n_m\psi(k_c(\lambda_p)R_c)\psi(k_m(\lambda_p)R_{sh})M_2 + n_c n_{sh}\psi(k_c(\lambda_p)R_c)\psi'(k_m(\lambda_p)R_{sh})M_3 + n_m n_{sh}\psi'(k_c(\lambda_p)R_c)\psi(k_m(\lambda_p)R_{sh})M_4 \quad (21)$$

$$X_4 = n_c n_{sh}(M_5 - M_6)\left[\xi(k_{sh}(\lambda_p)R_c)\psi'(k_{sh}(\lambda_p)R_c) - \xi'(k_{sh}(\lambda_p)R_c)\psi(k_{sh}(\lambda_p)R_c)\right] \quad (22)$$

$$X_5 = -n_{sh}\left\{\begin{array}{l} n_{sh}\psi'(k_c(\lambda_p)R_c)\left[\xi(k_{sh}(\lambda_p)R_c)M_5 - \xi(k_{sh}(\lambda_p)R_c)M_6\right] \\ +n_c\psi(k_c(\lambda_p)R_c)\left[\xi'(k_{sh}(\lambda_p)R_c)M_6 - \xi'(k_{sh}(\lambda_p)R_c)M_5\right] \end{array}\right\} \quad (23)$$

$$X_6 = -n_{sh}\left\{\begin{array}{l} n_{sh}\psi'(k_c(\lambda_p)R_c)\left[\psi(k_{sh}(\lambda_p)R_c)M_5 - \psi(k_{sh}(\lambda_p)R_c)M_6\right] \\ +n_c\psi(k_c(\lambda_p)R_c)\left[\psi'(k_{sh}(\lambda_p)R_c)M_6 - \psi'(k_{sh}(\lambda_p)R_c)M_5\right] \end{array}\right\} \quad (24)$$

$$X_7 = n_c n_m\psi'(k_c(\lambda_p)R_c)\psi'(k_m(\lambda_p)R_{sh})M_1 + n_{sh}n_m\psi(k_c(\lambda_p)R_c)\psi(k_m(\lambda_p)R_{sh})M_2 + n_{sh}^2\psi(k_c(\lambda_p)R_c)\psi'(k_m(\lambda_p)R_{sh})M_3 + n_c n_{sh}\psi'(k_c(\lambda_p)R_c)\psi(k_m(\lambda_p)R_{sh})M_4 \quad (25)$$

$$X_8 = -n_{sh}\left\{\begin{array}{l} n_c\psi'(k_c(\lambda_p)R_c)\left[\xi(k_{sh}(\lambda_p)R_c)M_5 - \xi(k_{sh}(\lambda_p)R_c)M_6\right] \\ +n_{sh}\psi(k_c(\lambda_p)R_c)\left[\xi'(k_{sh}(\lambda_p)R_c)M_6 - \xi'(k_{sh}(\lambda_p)R_c)M_5\right] \end{array}\right\} \quad (26)$$

$$X_9 = -n_{sh}\left\{\begin{array}{l} n_c\psi'(k_c(\lambda_p)R_c)\left[\psi(k_{sh}(\lambda_p)R_c)M_5 - \psi(k_{sh}(\lambda_p)R_c)M_6\right] \\ +n_{sh}\psi(k_c(\lambda_p)R_c)\left[\psi'(k_{sh}(\lambda_p)R_c)M_6 - \psi'(k_{sh}(\lambda_p)R_c)M_5\right] \end{array}\right\} \quad (27)$$

$$\begin{aligned} M_1 &= \xi(k_{sh}(\lambda_p)R_c)\psi(k_{sh}(\lambda_p)R_{sh}) - \xi(k_{sh}(\lambda_p)R_{sh})\psi(k_{sh}(\lambda_p)R_c); \\ M_2 &= \xi'(k_{sh}(\lambda_p)R_c)\psi'(k_{sh}(\lambda_p)R_{sh}) - \xi'(k_{sh}(\lambda_p)R_{sh})\psi'(k_{sh}(\lambda_p)R_c) \end{aligned} \quad (28)$$

$$\begin{aligned} M_3 &= \xi(k_{sh}(\lambda_p)R_{sh})\psi'(k_{sh}(\lambda_p)R_c) - \xi'(k_{sh}(\lambda_p)R_c)\psi(k_{sh}(\lambda_p)R_{sh}); \\ M_4 &= \xi'(k_{sh}(\lambda_p)R_{sh})\psi(k_{sh}(\lambda_p)R_c) - \xi(k_{sh}(\lambda_p)R_c)\psi'(k_{sh}(\lambda_p)R_{sh}) \end{aligned} \quad (29)$$

$$M_5 = \xi(k_m(\lambda_p)R_{sh})\psi'(k_m(\lambda_p)R_{sh}); M_6 = \xi'(k_m(\lambda_p)R_{sh})\psi(k_m(\lambda_p)R_{sh}) \quad (30)$$

where R_c and R_{sh} are the radii of the core and shell, respectively. k_m, k_{sh}, and k_c are the propagation constants of light in the surrounding medium, shell, and core, respectively. ξ_n and ψ_n are the Riccati-Hankel and Bessel functions, respectively[65]. τ_n and π_n are the angle-dependent associated Legendre polynomials, respectively. g_n is the correcting Bromwich coefficient, which is generally expressed as[21]

$$g_n = \frac{2n+1}{\pi n(n+1)}\frac{1}{(-1)^n i^n}\int_0^{\pi}\int_0^{\infty} ik_m r\sin^2\theta \times f \times \exp(-ik_m r\cos\theta)\psi_n^1(k_m r)P_n^1(\cos\theta)d\theta d(k_m r) \quad (31)$$

All parameters and functions in this expression are explained in Ref.[21]. Further, Gouesbet et al. simplified Eq. (31) as follows[66]

$$g_n = e^{-\rho_n^2/\omega_0^2} \quad (32)$$

here $\rho_n = (n+0.5)(\lambda/2\pi)$. It is to be noted that the Eq. (32) will be valid only when the center of the microsphere is located at the center of the beam waist (as in the present study).

The expression for $E_p(\lambda_p)$ is given below.

$$E_p(\lambda_p) = \frac{E_0(\lambda_p)}{\sum_{p=1}^{k} E_0(\lambda_p)}; \quad \sum_{p=1}^{k} E_p(\lambda_p) = 1 \quad (33)$$

here $E_0(\lambda_p)$ is the electric field amplitude of the radiation of wavelength λ_p.

It is important to note that all these equations are dependent on the refractive index (n) of the considered material. It is well known that the n value depends upon λ_p. In the case of polychromatic illumination, one has to consider the dispersion of the refractive index of the material. In the present study, polystyrene (PS) and fused silica have been considered as particle materials. The dispersion relations for PS[67] and fused silica[68] are given below in the same order.

$$n^2 - 1 = \frac{1.4435\lambda_p^2}{\lambda_p^2 - 0.020216} \quad (34)$$

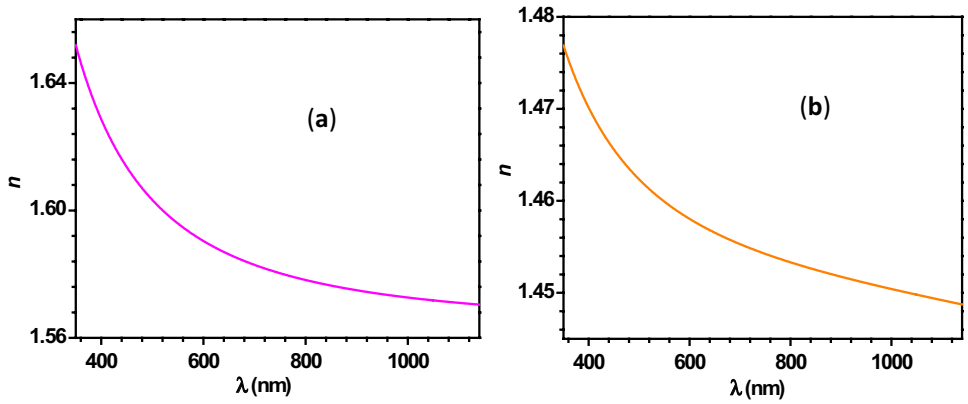

Figure 2. Panels (**a**,**b**) represent the dispersion of the refractive index of PS and fused silica, respectively.

$$n^2 - 1 = \frac{0.6961663\lambda_p^2}{\lambda_p^2 - 0.0684043^2} + \frac{0.4079426\lambda_p^2}{\lambda_p^2 - 0.1162414^2} + \frac{0.8974794\lambda_p^2}{\lambda_p^2 - 9.896161^2} \tag{35}$$

In addition, the dispersion curves for PS and fused silica are plotted using Eqs. (34 and 35) and shown in Fig. 2.

Results and discussion

Emission spectra of different polychromatic light sources. As mentioned in the introduction, the main aim of the present work is to understand the characteristic parameters of PNJs of single solid/core–shell microspheres under focused polychromatic illumination. So, to perform the theoretical investigation on PNJs of single dielectric microspheres using equations shown in the above section, the number of wavelengths present in the incident polychromatic light and electric field amplitude at each wavelength are necessary. These details can be obtained easily by recording the spectrum of polychromatic light. Therefore, before starting the theoretical investigation, the emission spectra of different polychromatic light sources such as Halogen lamp, white LED, SC source, and Hg arc lamp available in our laboratory are recorded using the charge-coupled device (CCD) spectrometer, and obtained spectra are used in the present study.

From Panel (a) of Fig. 3, it is clear that the spectrum of the Halogen lamp is continuous and spanned from 380 to 1000 nm. The peak maximum is observed at 640 nm. In the case of white LED, two peaks are observed. The central wavelengths of sharp and broad peaks are observed at 450 nm and 565 nm, respectively. In the case of SC source operated at lower power, the spectrum is started from 500 to 1100 nm. The supercontinuum radiation is generated from a photonic crystal fiber and a sharp peak in the spectrum at 1064 nm corresponds to the pump laser (i.e., picosecond diode laser). The background in the spectrum of the Hg arc lamp is spanned from 400 to 1100 nm. As expected, several sharp peaks are observed in the range from 380 to 600 nm.

PNJs generated by single PS microspheres kept in water medium. Using the spectra of different polychromatic light sources (Fig. 3) and theoretical equations mentioned in Sect. 2, the EFIE distribution inside and outside single PS microspheres is plotted and shown in Fig. 4.

In all panels, a white circle represents the microsphere boundary. The blue and red colors represent the lower and higher EFIE values. From this figure, it can be observed that the maximum EFIE (η_{max}) values obtained for all the mentioned light sources are not the same due to the difference in the wavelengths and electric field amplitude of the incident radiation. The PNJ generated through the microsphere due to the SC source illumination is the least convergent among all shown in the figure because the shorter wavelengths are not present in the spectrum. In addition, the radiation from the SC source contains several larger wavelengths (beyond 1000 nm). Since the spectrum of the LED contains one intense peak at a lower wavelength region, the η_{max} value observed for this source is slightly larger as compared to those obtained for other light sources.

Another characteristic parameter that plays a major role in several applications is the width of the PNJ. Therefore, the line scans along the transversal axis are taken across the PNJs generated using different light sources and shown in Fig. 5. In this figure, X = 0 indicates the center of the PNJs where the EFIE is maximum. The effective width of the PNJs (W_{eff}) is nothing but the width of the peaks. Here the W_{eff} is found smaller for the case of LED and it is larger for the SC source. It is worth mentioning here that the W_{eff} values are reasonably larger due to the smaller relative refractive index of the PS microspheres in the water medium. Therefore, these PNJs are not useful for some applications such as PNJ assisted super-resolution white light nanoscopy and photoacoustic spectroscopy. However, the W_{eff} can be lowered significantly in water medium if we use microspheres that have higher refractive indices.

As mentioned in the introduction, several researchers have numerically/theoretically studied the PNJs generated by single dielectric microparticles under monochromatic illumination. It has been reported that the characteristic parameters of the PNJs strongly depend upon the wavelength of the incident light, size, shape, and relative refractive index of the microparticles. In addition, there is always a little deviation between the

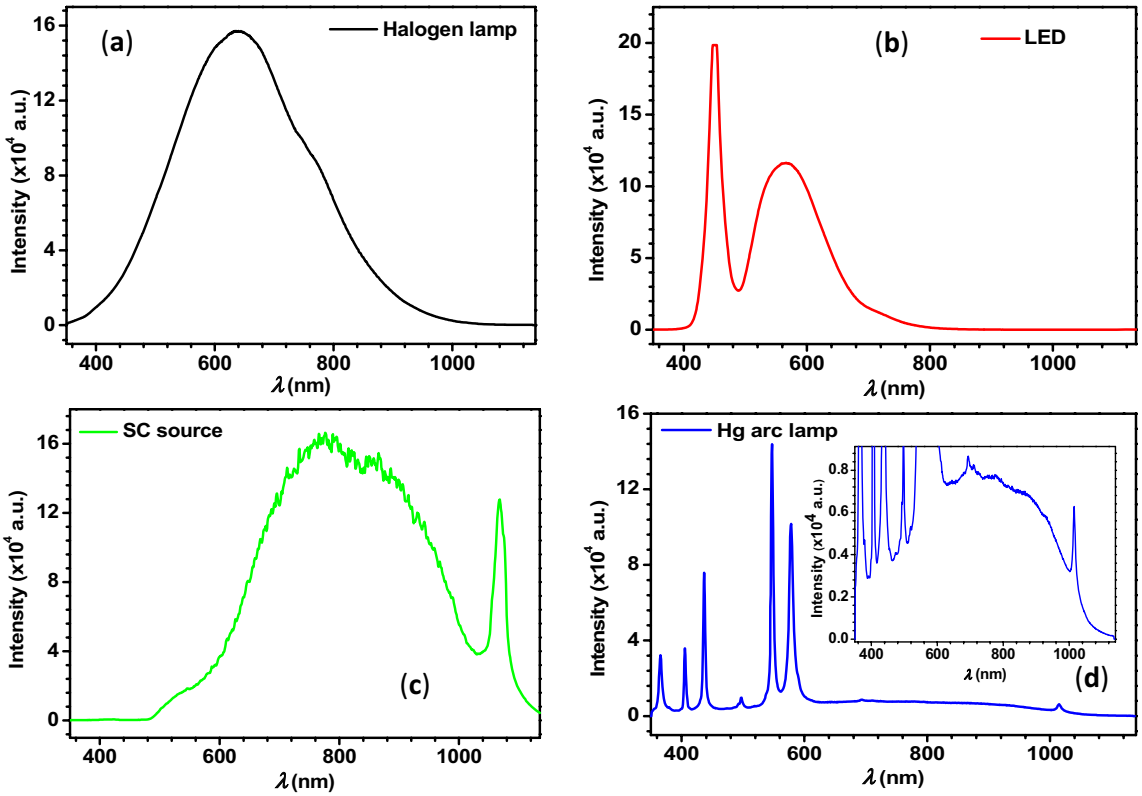

Figure 3. Panels (**a**–**d**) represent the spectra of Halogen lamp, white LED, SC source, and Hg arc lamp, respectively. Inset in panel (**d**) represents a portion of the vertically zoomed spectrum.

results obtained using different commercial software and theoretical approaches. Therefore, to have a proper comparison between the PNJs obtained by monochromatic and polychromatic illumination, we have performed the theoretical investigation on PNJ of single microspheres ($R_s = 3$ μm) illuminated by monochromatic light of different wavelengths and found that the η_{max} values obtained with monochromatic light of $\lambda = 655$ nm, Halogen lamp, and Hg arc lamp are quite close. To find out whether this is the same even for microspheres of different sizes or not, we have also estimated the η_{max} values for the microspheres of different sizes, illuminated by monochromatic light of $\lambda = 655$ nm, Halogen lamp, and Hg arc lamp and the obtained values are shown in panels (a) and (b) of Fig. 6, separately. In both the panels, overall, the η_{max} value is found to increase with the R_s value. This could be due to the predominant forward Mie scattering in the case of larger microspheres. It is to be noted that fluctuations in the curve for $\lambda = 655$ nm indicate the partial excitation of optical resonances or whispering gallery modes of the microspheres of specific sizes. From both the panels, we can conclude that the η_{max} values obtained for the Halogen light, Hg arc lamp, and monochromatic light of $\lambda = 655$ nm are nearby for all R_s values.

For comparing the W_{eff} values, the line scans along the transversal axes of the PNJs of the PS microsphere ($R_s = 3$ μm) illuminated by monochromatic light of $\lambda = 655$ nm, polychromatic light from Halogen lamp and Hg arc lamp are plotted and shown in panels (c) and (d) of Fig. 6. From these Panels, we can easily conclude that the W_{eff} values are also nearly the same.

For comparing the lengths of the PNJs, the line scans along the optical axes of the PNJs of the PS microsphere ($R_s = 3$ μm) illuminated by monochromatic light of $\lambda = 655$ nm, polychromatic light from Halogen lamp and Hg arc lamp are plotted and shown in panels (e) and (f) of Fig. 6. It is to be noted that the FWHM of the peaks shown in these two panels represents the effective length of the PNJs (L_{eff}). From these figures, it is clear that the L_{eff} is slightly more in the case of both polychromatic sources.

PNJs generated by single PS microspheres kept in air medium. Figure 7 shows the EFIE distribution inside and outside single PS microspheres (in air medium) illuminated by focused polychromatic light from different sources. As in the water medium, the η_{max} values obtained from the spectra of all polychromatic sources are slightly different. The η_{max} observed in the air medium is significantly larger as compared to those obtained in the water medium. This is due to the strong forward Mie scattering in the air medium due to the larger relative refractive index of the microsphere. Here also, (1) the η_{max} is larger in the case of white LED and it is smaller for the SC source, and (2) the width and length of the PNJs are significantly smaller in the air as compared to the water medium. Therefore, these PNJs could be recommended for PNJ assisted white light nanoscopy, photoacoustic spectroscopy, etc.

Figure 8 represents the line scans along the transversal axes of the PNJs shown in Fig. 7. In this figure also, X = 0 indicates the center of the PNJs where the EFIE is maximum. The width of the PNJs is nothing but the

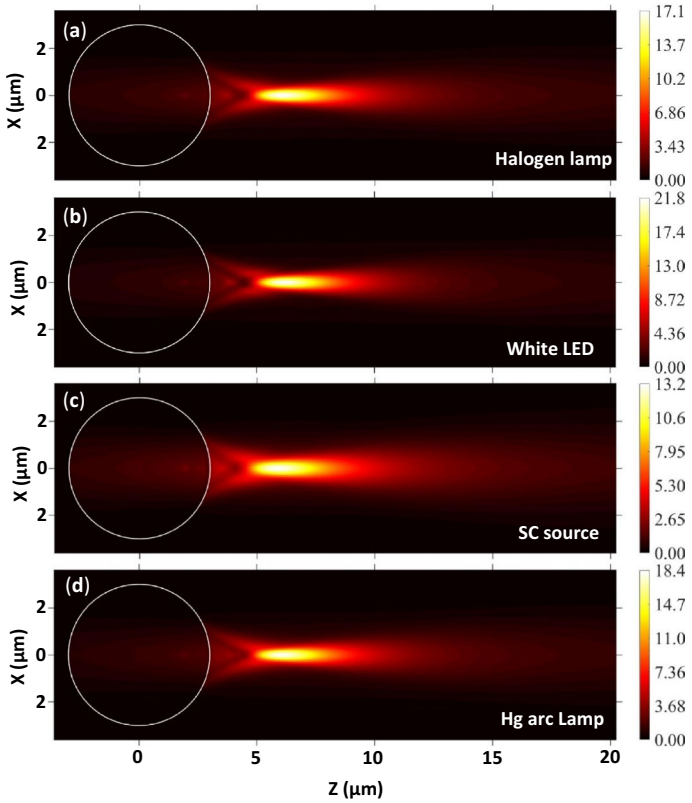

Figure 4. EFIE distribution inside and outside a PS microsphere illuminated by polychromatic light from different sources. Here $R_s = 3$ μm, $\omega_0 = 3$ μm, and $n_m = 1.333$. The wavelength-dependent refractive indices of PS are estimated from Eq. (34) and used for these simulations.

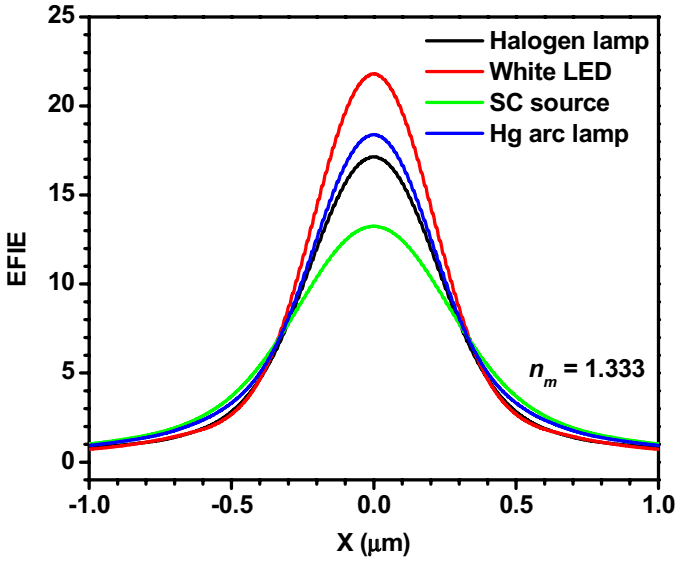

Figure 5. Variation in the EFIE along the transversal axes of the PNJs generated by a PS microsphere illuminated by polychromatic light from different sources. Here $R_s = 3$ μm, $\omega_0 = 3$ μm, and $n_m = 1.333$.

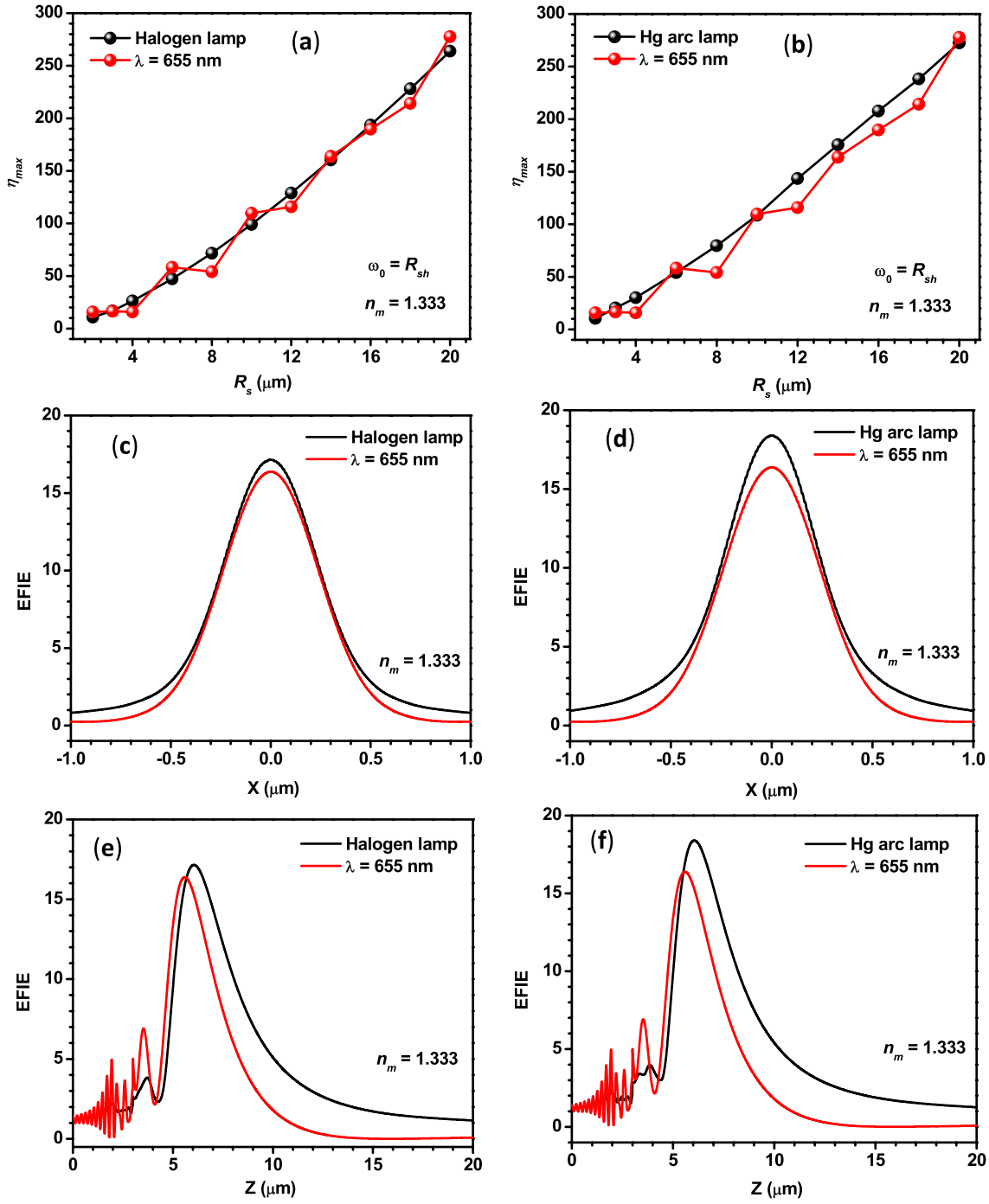

Figure 6. Panels (**a**,**b**) show the comparison between the η_{max} values obtained for monochromatic light of $\lambda = 655$ nm and polychromatic light from two different sources. Panels (**c**,**d**) show the comparison between the variation in the EFIE along the transversal axes of the PNJs generated by a PS microsphere illuminated by monochromatic light $\lambda = 655$ nm and polychromatic light from different sources. Panels (**e**,**f**) show the same along the longitudinal axes. In the case of the last four panels, $R_s = 3$ μm, and $\omega_0 = 3$ μm.

width of the peaks. It is apparent that only one peak is observed at X = 0 for all light sources but the side lobes are completely disappeared irrespective of the polychromatic light source. However, in the case of monochromatic illumination, along with the main peak at X = 0, several side lobes are observed in the air medium. The number and amplitude of the side lobes are significantly decreased when the λ value is increased from 400 to 1000 nm (results not shown). Here also, relatively, the width of the PNJ obtained for the SC source is slightly larger.

In the air medium also, at first, the EFIE distribution inside and outside a PS microsphere ($R_s = 3$ μm) is plotted using monochromatic light of different λ values. From Panels (a) and (b) of Fig. 9, it is apparent that the η_{max} values of microspheres having different R_s obtained for monochromatic light of $\lambda = 655$ nm, polychromatic light from Halogen and Hg arc lamps are nearly the same. In addition, from Panels (c–f) of Fig. 9, it can be observed

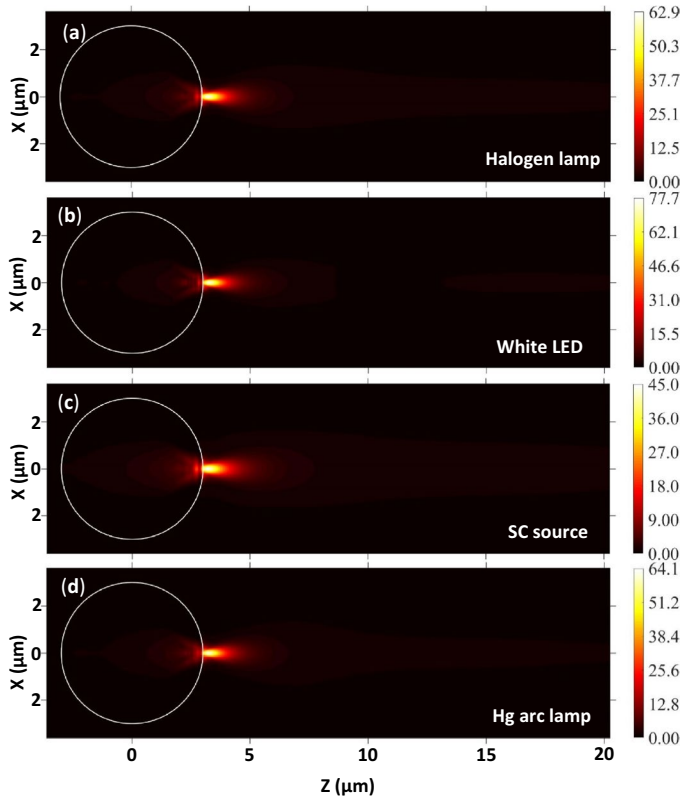

Figure 7. EFIE distribution inside and outside a PS microsphere illuminated by polychromatic light from different sources. Here $R_s = 3$ μm, $\omega_0 = 3$ μm, and $n_m = 1.0$.

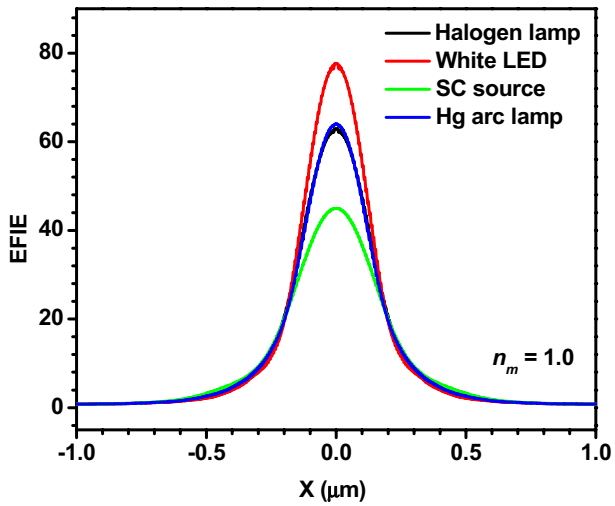

Figure 8. Variation in the EFIE along the transversal axes of the PNJ generated by a PS microsphere illuminated by polychromatic light from different sources. Here $R_s = 3$ μm, $\omega_0 = 3$ μm, and $n_m = 1.0$.

that the W_{eff} and L_{eff} values obtained for monochromatic light of $\lambda = 655$ nm, polychromatic light from Halogen and Hg arc lamps are close. Therefore, from Figs. (6 and 9), we can safely conclude that one can use the characteristic parameters of the PNJ obtained with monochromatic light of $\lambda = 655$ nm to interpret the experimental results obtained with the PNJs generated in air and water media, using the polychromatic light from Hg arc and Halogen lamps, which are the most commonly used in different types of microscopes. A similar observation is found for the silica microspheres as well (see "Supplementary information"). This observation is very useful for

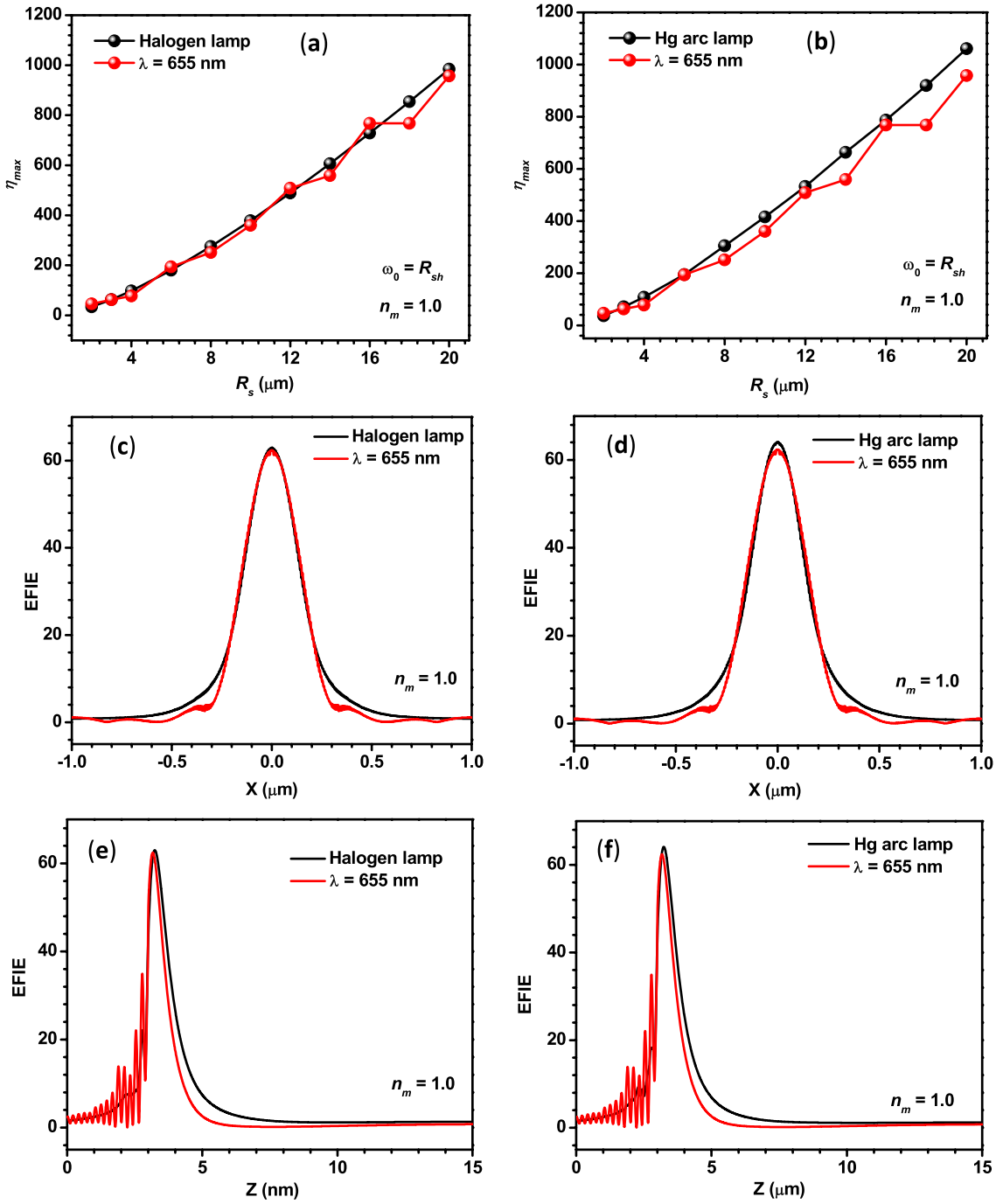

Figure 9. Panels (**a**,**b**) show the comparison between the η_{max} values obtained for monochromatic light of λ = 655 nm and polychromatic light from two different sources. Panels (**c**,**d**) show the comparison between the variation in the EFIE along the transversal axes of the PNJs generated by a PS microsphere illuminated by monochromatic light of λ = 655 nm and polychromatic light from different sources. Panels (**e**,**f**) show the same along the longitudinal axes. In the case of the last four panels, $R_s = 3$ μm, and $\omega_0 = 3$ μm.

the researchers because generating PNJs numerically using monochromatic light is simple but the generation of PNJs numerically using polychromatic light is a difficult task and it demands a sophisticated computing facility.

A comparison between the EFIE distribution of the PNJs obtained from the PS microsphere under the illumination of polychromatic light from a white LED and SC source with the monochromatic light of different wavelengths is also made for finding the suitable wavelength of monochromatic radiation.

It can be observed from Panels (a) and (c) of Fig. 10 that the W_{eff} and L_{eff} values obtained for monochromatic light of λ = 630 nm and polychromatic light from LED are very close. Similar behavior can be observed from Panels (b) and (d) of Fig. 10 for monochromatic light of λ = 800 nm and polychromatic light from SC source. Thus, the characteristic parameters of the PNJs obtained from the illumination of the monochromatic light of

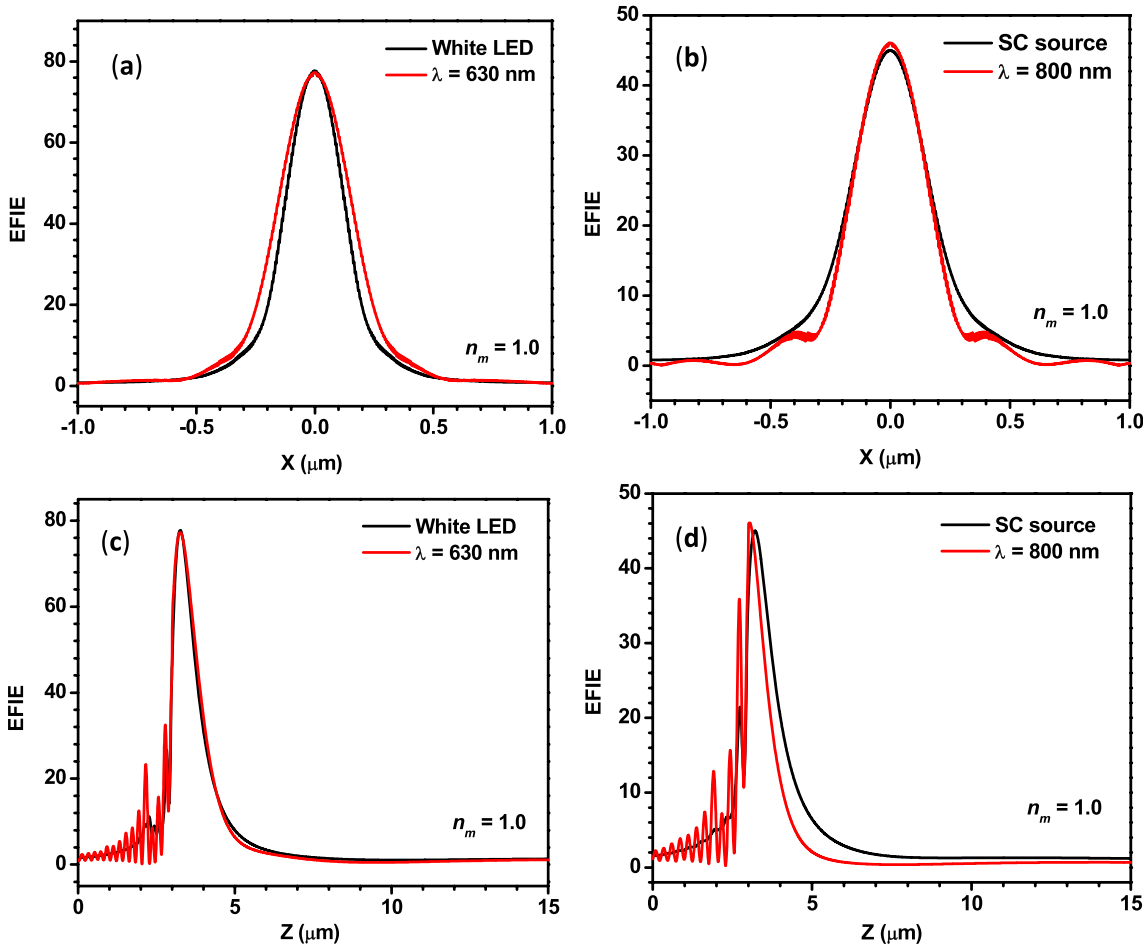

Figure 10. Panels (**a**,**b**) show the comparison between the variation in the EFIE along the transversal axes of the PNJs generated by a PS microsphere illuminated by monochromatic and polychromatic light from different sources. Panels (**c**,**d**) show the same along the longitudinal axes. For all the four panels, $R_s = 3$ μm and $\omega_0 = 3$ μm.

the mentioned wavelengths can be used to interpret the experimental results for the PNJs under the illumination by respective polychromatic light sources as mentioned earlier in this section.

Role of ω_0 on the PNJs of single microspheres under polychromatic illumination. Experimentally, the PNJs are generated by focusing the polychromatic light on single microspheres with the help of a microscopic objective lens with different numerical aperture (NA) values. It is well known that the NA value directly affects the ω_0. Though, the effect of ω_0 on the EFIE of the PNJ due to monochromatic illumination is reported in the literature[69], the same due to the polychromatic illumination is again not present in the literature. Therefore, to understand the effect of ω_0 on the PNJs of single microspheres under polychromatic illumination theoretically, the EFIE distribution inside and outside single microspheres is plotted by varying the ω_0 value. Figure 11 shows the EFIE distribution of a single PS microsphere of $R_s = 3$ μm obtained for different ω_0 values. Here the emission spectrum of Halogen light shown in panel (a) of Fig. 3 is used for generating all panels in Fig. 11.

From Fig. 11, it can be observed that for a very small ω_0 (= 0.5 μm) compared to the size of the microsphere, there is no formation of PNJ. The incident light is focused at the centre of the microsphere. When $\omega_0 = 1$ μm then the PNJ is partially visible outside the microsphere. But a reasonable amount of light is still confined inside the microsphere. Upon increasing the ω_0 value from 1 to 2 μm, the PNJ is clearly visible outside the microsphere. However, the value of η_{max} is low due to the weak confinement of the PNJ. When $\omega_0 = R_s$, the value of η_{max} is increased further which indicates the improvement in the confinement of PNJ. These results indicate that one has to use the focused polychromatic beam with $\omega_0 = R_s$ to generate the tightly confined PNJs from single dielectric microspheres.

PNJs generated by silica core-PS shell microspheres kept in air medium. The theoretical investigation is extended for studying the PNJs of core–shell microspheres illuminated by polychromatic light. Panels (a) and (b) of Fig. 12 show the EFIE distribution of single silica core-PS shell microspheres obtained using the spectra of Halogen lamp and Hg arc lamp, respectively. From these two panels, it is clear that only one PNJ is observed in all the cases due to the thin shell. In general, several short and elongated PNJs are expected in the case of a thicker shell on a large sphere[59] or multi-shells on a solid sphere[70] due to multiple focusing and defocus-

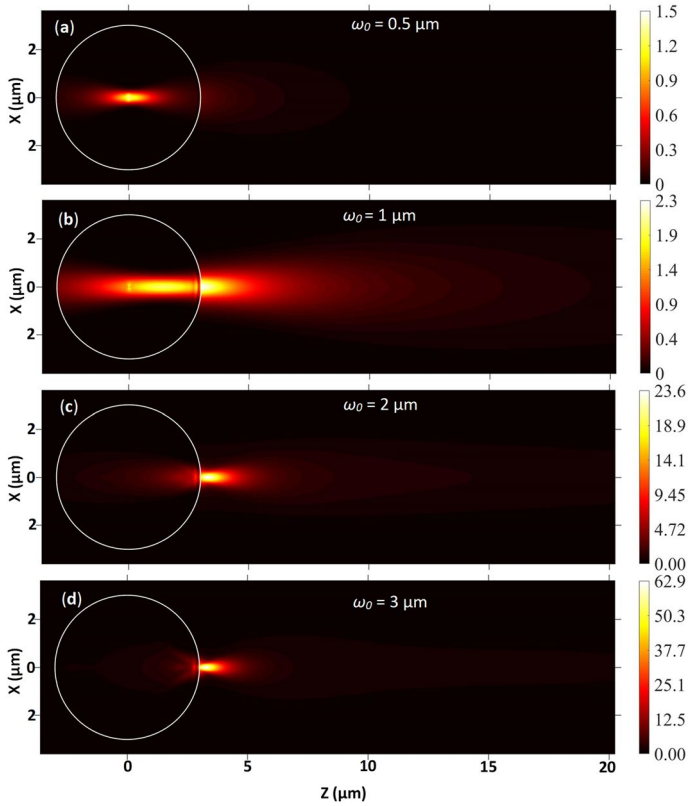

Figure 11. The role of ω_0 on the EFIE inside and outside a PS microsphere illuminated by focused polychromatic light. Here $R_s = 3$ µm and $n_m = 1.0$. The spectrum of the Halogen lamp is used for generating all figures.

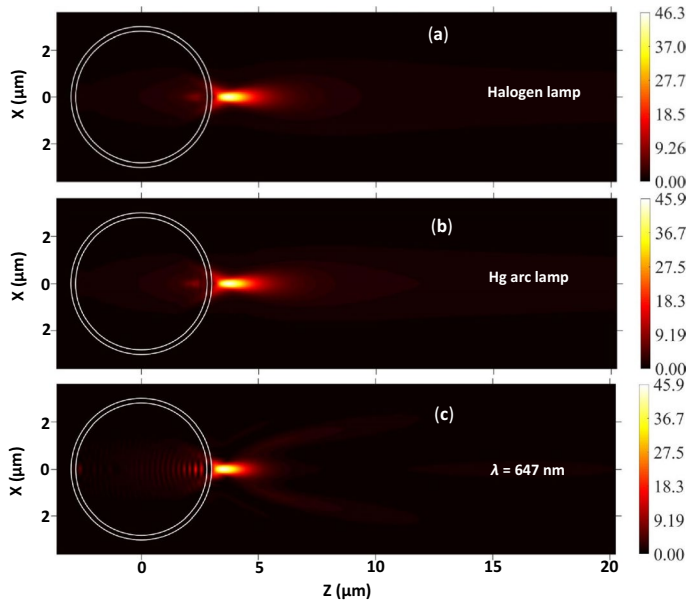

Figure 12. (**a**–**c**) represent the EFIE distribution inside and outside a silica core-PS shell microsphere illuminated by a Halogen lamp, Hg arc lamp, and monochromatic light of λ = 647 nm, respectively. For all the panels, $R_c = 2.8$ µm, $R_{sh} = 3.0$ µm, $\omega_0 = 3$ µm, and $n_m = 1.0$. The wavelength-dependent refractive indices of the PS and silica are estimated using Eqs. (34 and 35), respectively, and the obtained values are used for these simulations.

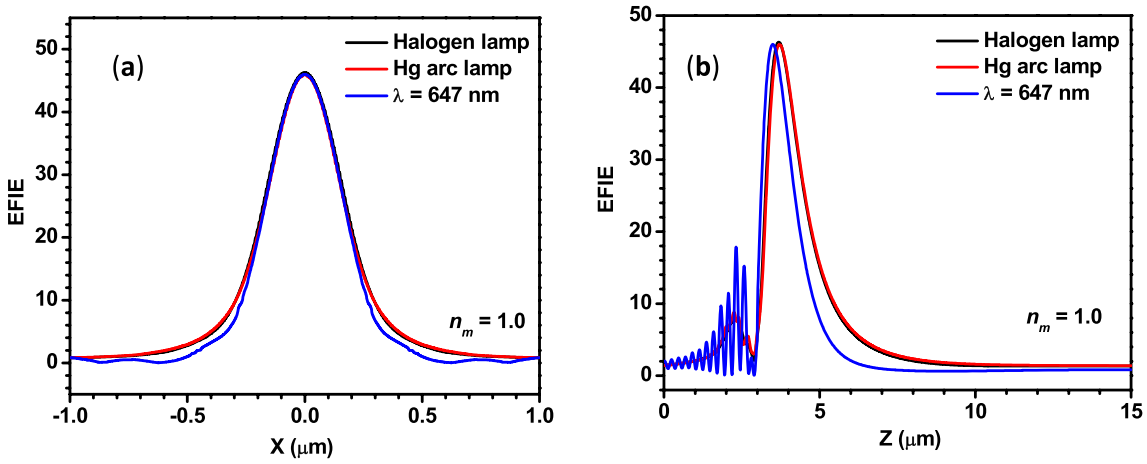

Figure 13. The variation in the EFIE along the transversal and longitudinal axes of the PNJs are shown in panels (**a**,**b**), respectively. For both the panels, $R_c = 2.8$ μm, $R_{sh} = 3.0$ μm, $\omega_0 = 3$ μm, and $n_m = 1.0$.

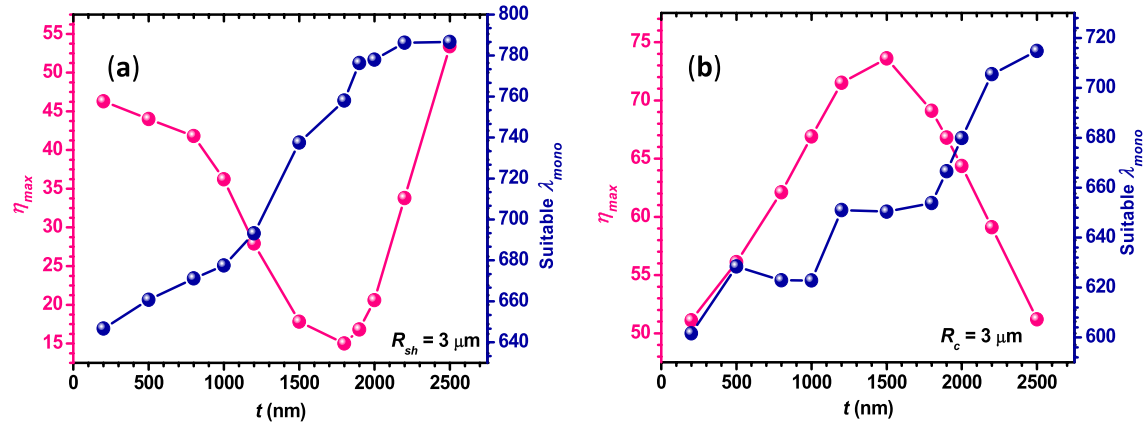

Figure 14. The pink curves in both the panels show the variation of η_{max} with t value in the case of polychromatic light from the Halogen lamp. The blue curves in both panels represent the variation of suitable λ_{mono} with the t value. For panels (**a**,**b**), the t value is varied by fixing the R_{sh} and R_c value, respectively. For all cases, $\omega_0 = R_{sh}$ and $n_m = 1.0$.

ing of the incident light. The η_{max} value found in the present case is lower than that obtained in the case of a solid PS microsphere of $R_s = 3$ μm. In the above sections, it is mentioned that the characteristic parameters of the PNJs of single solid microspheres obtained using the spectra of Halogen and Hg arc lamps are close to those obtained with the monochromatic light of $\lambda = 655$ nm. To find out the suitable wavelength of monochromatic radiation (λ_{mono}) for the present case also, the EFIE distribution is plotted inside and outside the core–shell microspheres illuminated by monochromatic radiation of different wavelengths. From Figs. 12 and 13, it is clear that the η_{max}, W_{eff}, and L_{eff} of the PNJs generated by core–shell microsphere under illumination with polychromatic radiation and monochromatic radiation of $\lambda = 647$ nm are very close. From these results, we can also conclude that one can use the characteristic parameters of the PNJ of core–shell microspheres (having thin shells) obtained with monochromatic light of $\lambda = 647$ nm to interpret the experimental results obtained with the PNJs of core–shell microspheres generated by polychromatic light from Halogen and Hg arc lamps.

The effect of shell thickness (t) on the characteristic parameters of the PNJs is also investigated theoretically. The pink curve in panel (a) of Fig. 14 represents the variation of η_{max} with the t value in the case of polychromatic radiation from the Halogen lamp. Here the t value is increased by fixing the value of R_{sh} at 3 μm and varying the R_c value from 2.8 to 0.5 μm. In this case, the value of η_{max} is found to decrease upon increasing the t value till 1800 nm. Beyond this t value, η_{max} is found to increase. For each t value, the suitable λ_{mono} has been found to generate the PNJ which has the characteristic parameters close to those obtained in the case of polychromatic radiation and mentioned in the same panel (blue color curve). In this case, the suitable λ_{mono} value is found to show an overall increase with t. When the t value is varied by fixing the R_c value at 3 μm and varying the R_{sh} value from 3.2 to 5.5 μm, the η_{max} is observed to follow the reverse trend in the case of polychromatic illumination [panel (b) of Fig. 14] in contrast to the previous case [panel (a)]. However, the suitable λ_{mono} value is again found to increase overall with the t value.

Conclusions

The analytical equations which are useful to understand the characteristic parameters of the PNJs of single microspheres under polychromatic illumination are given in this paper. For the first time, a theoretical investigation is carried out on the PNJs generated using the emission spectra of Halogen lamp, SC source, white LED, and Hg arc lamp. For better comparison, the PNJs are also generated theoretically using monochromatic light of different λ values. The η_{max}, $W_{eff,}$ and L_{eff} of the PNJ obtained for all the polychromatic sources are slightly different due to the variation in the emission spectra. Relatively, the η_{max} is little larger, W_{eff} and L_{eff} values are slightly smaller in the case of white LED. These are found to be opposite in the case of SC source. The characteristic parameters of the PNJs of microspheres under polychromatic illumination are found sensitive with the R_s and n_m as in the case of monochromatic illumination. More importantly, the characteristic parameters of the PNJs of solid microspheres obtained for all polychromatic light sources are found close to those observed for the monochromatic light of λ which is near to the central wavelength of the polychromatic light sources. This means one can use the characteristic parameters of the PNJ of the solid microspheres observed with monochromatic light with suitable λ to interpret the experimental results obtained with the PNJs generated by polychromatic light from the above-mentioned sources.

In the case of core–shell microspheres, the characteristic parameters of the PNJs obtained with polychromatic light are sensitivity to the t value as in the case of monochromatic illumination. In addition, the suitable λ_{mono} values are found to increase with t values. We believe that the observations reported here are very useful for the researchers because generating PNJs numerically using monochromatic light is simple but the generation of PNJs numerically using polychromatic light is a difficult task and it demands a sophisticated computing facility.

Received: 11 July 2021; Accepted: 30 November 2021
Published online: 07 January 2022

References

1. Matsko, A. B. & Ilchenko, V. S. Optical resonators with whispering-gallery modes-part I: Basics. *IEEE J. Sel. Top. Quantum Electron.* **12**(1), 3–14 (2006).
2. Teraoka, I., Arnold, S. & Vollmer, F. Perturbation approach to resonance shifts of whispering-gallery modes in a dielectric microsphere as a probe of a surrounding medium. *J. Opt. Soc. Am. B* **20**(9), 1937–1946 (2003).
3. Vahala, K. J. Optical microcavities. *Nature* **424**(6950), 839–846 (2003).
4. Serpengüzel, A., Arnold, S. & Griffel, G. Excitation of resonances of microspheres on an optical fiber. *Opt. Lett.* **20**(7), 654–656 (1995).
5. Kosma, K., Zito, G., Schuster, K. & Pissadakis, S. Whispering gallery mode microsphere resonator integrated inside a microstructured optical fiber. *Opt. Lett.* **38**(8), 1301–1303 (2013).
6. Buck, J. R. & Kimble, H. J. Optimal sizes of dielectric microspheres for cavity QED with strong coupling. *Phys. Rev. A* **67**(3), 033806 (2003).
7. Dantham, V. R., Holler, S., Kolchenko, V., Wan, Z. & Arnold, S. Taking whispering gallery-mode single virus detection and sizing to the limit. *Appl. Phys. Lett.* **101**(4), 043704 (2012).
8. Dantham, V. R. *et al.* Label-free detection of single protein using a nanoplasmonic-photonic hybrid microcavity. *Nano Lett.* **13**(7), 3347–3351 (2013).
9. Yue, L. *et al.* Super-enhancement focusing of teflon spheres. *Ann. Phys.* **532**(10), 2000373 (2020).
10. Wang, Z. *et al.* High order fano resonances and giant magnetic fields in dielectric microspheres. *Sci. Rep.* **9**(1), 1–7 (2019).
11. Heifetz, A., Kong, S. C., Sahakian, A. V., Taflove, A. & Backman, V. Photonic nanojets. *J. Comput. Theor. Nanosci.* **6**(9), 1979–1992 (2009).
12. Itagi, A. V. & Challener, W. A. Optics of photonic nanojets. *J. Opt. Soc. Am. A* **22**(12), 2847–2858 (2005).
13. Lee, S., Li, L. & Wang, Z. Optical resonances in microsphere photonic nanojets. *J. Opt.* **16**(1), 015704 (2013).
14. Kim, M. S., Scharf, T., Mühlig, S., Rockstuhl, C. & Herzig, H. P. Engineering photonic nanojets. *Opt. Expr.* **19**(11), 10206–10220 (2011).
15. Luk'yanchuk, B. S., Paniagua-Domínguez, R., Minin, I., Minin, O. & Wang, Z. Refractive index less than two: Photonic nanojets yesterday, today and tomorrow. *Opt. Mater. Expr.* **7**(6), 1820–1847 (2017).
16. Zhu, J. & Goddard, L. L. All-dielectric concentration of electromagnetic fields at the nanoscale: The role of photonic nanojets. *Nanoscale Adv.* **1**(12), 4615–4643 (2019).
17. Chen, Z., Taflove, A. & Backman, V. Photonic nanojet enhancement of backscattering of light by nanoparticles: A potential novel visible-light ultramicroscopy technique. *Opt. Expr.* **12**(7), 1214–1220 (2004).
18. Ferrand, P. *et al.* Direct imaging of photonic nanojets. *Opt. Expr.* **16**(10), 6930–6940 (2008).
19. Liu, Y. *et al.* Characteristics of photonic nanojets from two-layer dielectric hemisphere. *Chin. Phys. B* **26**(11), 114201 (2017).
20. Kim, M. S., Scharf, T., Mühlig, S., Rockstuhl, C. & Herzig, H. P. Engineering photonic nanojets. *Opt. Expr.* **19**(11), 10206–10220 (2011).
21. Mandal, A. & Dantham, V. R. Photonic nanojets generated by single microspheres of various sizes illuminated by resonant and non-resonant focused Gaussian beams of different waists. *J. Opt. Soc. Am. B* **37**(4), 977–986 (2020).
22. Han, L., Han, Y., Gouesbet, G., Wang, J. & Gréhan, G. Photonic jet generated by spheroidal particle with Gaussian-beam illumination. *J. Opt. Soc. Am. B* **31**(7), 1476–1483 (2014).
23. Grojo, D. *et al.* Bessel-like photonic nanojets from core-shell sub-wavelength spheres. *Opt. Lett.* **39**(13), 3989–3992 (2014).
24. Jia, Y., Li, R., Zhuang, W. & Liang, J. Photonic nanojet generated by a spheroidal particle illuminated by a vector Bessel beam. *Res. Opt.* **4**, 100106 (2021).
25. Kiselev, A. D. & Plutenko, D. O. Mie scattering of Laguerre-Gaussian beams: Photonic nanojets and near-field optical vortices. *Phys. Rev. A* **89**(4), 043803 (2014).
26. Neves, A. A. R. Photonic nanojets in optical tweezers. *J. Quant. Spectrosc. Radiat. Transfer* **162**, 122–132 (2015).
27. Wannaprapa, M. (2014). The characterization of microspherical particle by light scattering theory using near field: photonic nanojets (Doctoral dissertation, Faculty of Engineering, Thammasat University).
28. Dantham, V. R., Bisht, P. B. & Namboodiri, C. K. R. Enhancement of Raman scattering by two orders of magnitude using photonic nanojet of a microsphere. *J. Appl. Phys.* **109**(10), 103103 (2011).
29. Arya, A., Laha, R., Das, G. M. & Dantham, V. R. Enhancement of Raman scattering signal using photonic nanojet of portable and reusable single microstructures. *J. Raman Spectrosc.* **49**(5), 897–902 (2018).

30. Das, G. M., Laha, R. & Dantham, V. R. Photonic nanojet-mediated SERS technique for enhancing the Raman scattering of a few molecules. *J. Raman Spectrosc.* **47**(8), 895–900 (2016).
31. Das, G. M., Ringne, A. B., Dantham, V. R., Easwaran, R. K. & Laha, R. Numerical investigations on photonic nanojet mediated surface-enhanced Raman scattering and fluorescence techniques. *Opt. Expr.* **25**(17), 19822–19831 (2017).
32. Sergeeva, K. A. *et al.* Highly-sensitive fluorescent detection of chemical compounds Via photonic nanojet excitation. *Sens. Actuators B: Chem.* **305**, 127354 (2020).
33. Gu, G. *et al.* Single nanoparticle detection using a photonic nanojet. *Nanoscale* **10**(29), 14182–14189 (2018).
34. Kong, S. C., Sahakian, A., Taflove, A. & Backman, V. Photonic nanojet-enabled optical data storage. *Opt. Expr.* **16**(18), 13713–13719 (2008).
35. Astratov, V. N. *et al.* Photonic nanojets for laser surgery. *SPIE Newsroom* **12**, 32–34 (2010).
36. Darafsheh, A. Photonic nanojets and their applications. *J. Phys.: Photon.* **3**(2), 022001 (2021).
37. Lecler, S. *et al.* Photonic jet driven non-linear optics: example of two-photon fluorescence enhancement by dielectric microspheres. *Opt. Expr.* **15**(8), 4935–4942 (2007).
38. Zhang, X. A., Chen, I. T. & Chang, C. H. Recent progress in near-field nanolithography using light interactions with colloidal particles: From nanospheres to three-dimensional nanostructures. *Nanotechnology* **30**(35), 352002 (2019).
39. Surdo, S., Duocastella, M. & Diaspro, A. Nanopatterning with photonic nanojets: Review and perspectives in biomedical research. *Micromachines* **12**(3), 256 (2021).
40. Yang, S., Taflove, A. & Backman, V. Experimental confirmation at visible light wavelengths of the backscattering enhancement phenomenon of the photonic nanojet. *Opt. Expr.* **19**(8), 7084–7093 (2011).
41. Upputuri, P. K., Krisnan, M. S., Moothanchery, M., & Pramanik, M. (2017). Photonic nanojet engineering to achieve super-resolution in photoacoustic microscopy: a simulation study. In Photons Plus Ultrasound: Imaging and Sensing 2017 (Vol. 10064, p. 100644S). *International Society for Optics and Photonics*.
42. Lee, S. & Li, L. Rapid super-resolution imaging of sub-surface nanostructures beyond diffraction limit by high refractive index microsphere optical nanoscopy. *Opt. Commun.* **334**, 253–257 (2015).
43. Upputuri, P. K. & Pramanik, M. Microsphere-aided optical microscopy and its applications for super-resolution imaging. *Opt. Commun.* **404**, 32–41 (2017).
44. Liu, C. & Ye, A. Microsphere-assisted optical super-resolution imaging with narrowband illumination. *Opt. Commun.* **485**, 126658 (2021).
45. Perrin, S., Lecler, S., Leong-Hoi, A., & Montgomery, P. C. (2017). Role of coherence in microsphere-assisted nanoscopy. In Modeling Aspects in Optical Metrology VI (Vol. 10330, p. 103300V). *International Society for Optics and Photonics*.
46. Ling, J., Wang, X., Li, D. & Liu, X. Modeling and verification of white light oil immersion microsphere optical nanoscope. *Opt. Quantum Electron.* **49**(11), 1–11 (2017).
47. Li, L., Guo, W., Yan, Y., Lee, S. & Wang, T. Label-free super-resolution imaging of adenoviruses by submerged microsphere optical nanoscopy. *Light: Sci. Appl.* **2**(9), e104–e104 (2013).
48. Wang, Z. *et al.* Optical virtual imaging at 50 nm lateral resolution with a white-light nanoscope. *Nat. Commun.* **2**(1), 1–6 (2011).
49. Li, Y., Liu, X. & Li, B. Single-cell biomagnifier for optical nanoscopes and nanotweezers. *Light: Sci Appl* **8**(1), 1–12 (2019).
50. Perrin, S., Lecler, S., & Montgomery, P. (2019). Microsphere-assisted interference microscopy. *Label-Free Super-Resolution Microscopy* (pp. 443–469). Springer.
51. Kassamakov, I. *et al.* 3D super-resolution optical profiling using microsphere enhanced Mirau interferometry. *Sci. Rep.* **7**(1), 1–7 (2017).
52. Maconi, G., Kassamakov, I., Vainikka, T., Arstila, T., & Hæggström, E. (2019). Light-sample interaction in microsphere enhanced 2D super-resolution imaging. In Optical Measurement Systems for Industrial Inspection XI (Vol. 11056, p. 110560Q). *International Society for Optics and Photonics*.
53. Huszka, G., Yang, H. & Gijs, M. A. Microsphere-based super-resolution scanning optical microscope. *Opt. Expr.* **25**(13), 15079–15092 (2017).
54. Zhou, Y., Tang, Y., He, Y., Liu, X. & Hu, S. Effects of immersion depth on super-resolution properties of index-different microsphere-assisted nanoimaging. *Appl. Phys. Expr.* **11**(3), 032501 (2018).
55. Geints, Y. E., Panina, E. K. & Zemlyanov, A. A. Control over parameters of photonic nanojets of dielectric microspheres. *Opt. Commun.* **283**(23), 4775–4781 (2010).
56. Lee, S., Li, L. & Wang, Z. Optical resonances in microsphere photonic nanojets. *J. Opt.* **16**(1), 015704 (2013).
57. Lecler, S., Takakura, Y. & Meyrueis, P. Properties of a three-dimensional photonic jet. *Opt. Lett.* **30**(19), 2641–2643 (2005).
58. Yousefi, M., Scharf, T. & Rossi, M. Photonic nanojet generation under converging and diverging beams. *J. Opt. Soc. Am. B* **38**(2), 317–326 (2021).
59. Mandal, A. & Dantham, V. R. Short and elongated photonic nanojets emerged from single solid/hollow core-shell microparticles illuminated by focused Gaussian beams and plane wave. *J. Quant. Spectrosc. Radiat. Trans.* **257**, 107350 (2020).
60. Geints, Y. E., Zemlyanov, A. A. & Panina, E. K. Temporal dynamics of a "Photonic Jet" from a dielectric microparticle illuminated by a laser pulse. *Atmos. Ocean. Opt.* **26**(4), 259–264 (2013).
61. Geints, Y. E., Zemlyanov, A. A., & Panina, E. K. (2014). Extremal localization of optical field near surface of spherical dielectric microparticles. In 20th International Symposium on Atmospheric and Ocean Optics: Atmospheric Physics (Vol. 9292, p. 92921A). *International Society for Optics and Photonics*.
62. Uenohara, T., Takaya, Y. & Mizutani, Y. Laser micro machining beyond the diffraction limit using a photonic nanojet. *CIRP Ann. Manuf. Technol.* **66**(1), 491–494 (2017).
63. Pichette, C., Piché, M., Marquet, P., & Thibault, S. (2018). Temporal study of photonic jet formations under ultrashort laser pulses illumination for different geometries in near-field optical microscopy. *Imaging Systems and Applications* (pp. ITu3B-4). Optical Society of America.
64. Rudenko, A. & Moloney, J. V. Tunable near-to far-infrared optical breakdown in nonlinear interactions of ultrashort laser pulses with water microdroplets in ambient air. *Adv. Photon. Res.* **1**(2), 2000029 (2020).
65. Bohren, C. F. & Huffman, D. R. *Absorption and scattering of light by small particles* (Wiley, 2008).
66. Gouesbet, G., Gréhan, G. & Maheu, B. Scattering of a Gaussian beam by a Mie scatter center using a Bromwich formalism. *J. Opt.* **16**(2), 83 (1985).
67. Sultanova, N., Kasarova, S. & Nikolov, I. Dispersion properties of optical polymers. *Acta Phys. Polonica-Ser. A General Phys.* **116**(4), 585 (2009).
68. Malitson, I. H. Interspecimen comparison of the refractive index of fused silica. *J. Opt. Soc. Am.* **55**, 1205–1208 (1965).
69. Geynts, Y. E., Zemlyanov, A. A. & Panina, E. K. Features of photonic nanojet formation near surfaces of spherical microparticles illuminated by a focused laser beam. *Atmos. Ocean. Opt.* **28**(2), 139–144 (2015).
70. Geints, Y. E., Zemlyanov, A. A. & Panina, E. K. Photonic nanojet calculations in layered radially inhomogeneous micrometer-sized spherical particles. *J. Opt. Soc. Am. B* **28**(8), 1825–1830 (2011).

Author contributions

The concept was conceived by P.K.U. and V.R.D. The analytical equations and MATLAB programs were developed by A.M. The theoretical simulations were performed by P.T. Results were analysed by P.T and V.R.D. All authors have contributed to the writing of the manuscript. The overall work was supervised by V.R.D.

Competing interests

The authors declare no competing interests.

Additional information

Supplementary Information The online version contains supplementary material available at https://doi.org/10.1038/s41598-021-03610-3.

Correspondence and requests for materials should be addressed to V.R.D.

Reprints and permissions information is available at www.nature.com/reprints.

Publisher's note Springer Nature remains neutral with regard to jurisdictional claims in published maps and institutional affiliations.